Pergamon

Cement and Concrete Research 30 (2000) 521–527

CEMENT AND CONCRETE RESEARCH

Mercury intrusion porosimetry and hierarchical structure of cement pastes Theory and experiment

Radim Vočka[a], Christophe Gallé[b], Marc Dubois[a,*], Patrick Lovera[b]

[a]CEA, Service de Physique de l'Etat Condensé, F-91191 Gif-sur-Yvette, France
[b]CEA, Service d'études d'Entreposage et de Stockage des Déchets, F-91191 Gif-sur-Yvette, France

Received 18 May 1999; accepted 1 December 1999

Abstract

We developed a mercury intrusion porosimetry (MIP) simulator that takes into account the hierarchical structure of the porosity in certain materials (e.g., cement paste). We show that pore diameters indicated by the MIP results depend not only on the pore size distribution in the sample, but also on the connectivity of the pore space. On the basis of our simulations, we interpret experimental data obtained for cement pastes with and without a reactive admixture. The MIP data show that the capillary porosity for the pure paste is connected, even for the water/cement ratio w/c = 0.30, at variance with the Powers-Brownyard model of hydration. Our experimental results are in accordance with observations that the hydration process fixes the morphology of the hydration product. This morphology does not evolve continuously with w/c, only with the fraction of C-S-H corresponding to a given morphology evolves.

Keywords: Pore size distribution; Cement paste; Modeling

1. Introduction

Mercury intrusion porosimetry (MIP) is a widely used method for measuring the pore size distribution in porous media. It is based on the fact that for squeezing out a nonwetting fluid in a pore of the diameter d, a pressure P inversely proportional to the diameter of this pore must be applied. For a cylindrical pore this pressure is given by the Washburn (Laplace) relation, as seen in Eq. (1):

$$P = -4\gamma\cos\Theta/d \quad (1)$$

where γ is the surface energy of the liquid and Θ is the contact angle. The fraction of porosity occupied by pores having diameters in the interval $(d; d + \delta d)$ is then deduced from the volume of mercury intruded in the pressure range $(P; P + \delta P)$, supposing that all the pores are directly connected to the source of mercury. As this hypothesis is not generally verified, it turns out that the measured and the real pore size distributions differ significantly. In fact a pore of diameter d accessible only through pores of smaller diameters $d' < d$ ("hidden" pore) contributes to the porosity related to a diameter d'.

Several types of the mercury intrusion simulators have been developed to reach a better understanding of this phenomena. One of the oldest ideas was to represent a structure of a porous solid as a random packing of spheres [1,2]. This approach is suitable for sandstone and unconsolidated media, but it is not sufficiently general. An important number of simulators were built on the "pore network" models [3–5]. Pores, represented as tubes of a given diameter, are distributed over a regular network (Fig. 1). These models are rather simple, but they contain all the necessary ingredients for a correct qualitative description of the transport in porous media. A simple variation of these are so called "pore-throat" models, where the nodes of the network represent pores, which are connected by a narrow cylindrical throats [6]. The throats control the invasion, and the pores the retraction. Simulators have been devised where not only the diameter but also an exact form of pores and throats was taken into account [7]. An advantage of the pore network models is that they can be treated using the tools of percolation theory [8].

In this context should be mentioned the work of Larson and Morrow [9], who developed a simulator based on Bethe lattice (tree-shaped network with a fixed connectivity). The percolation problem on the Bethe lattice is exactly soluble, so this model permits an analytical treatment.

* Corresponding author. Tel.: +33-69-08-74-18; fax: +33-69-08-87-86.
E-mail address: mad@spec.saclay.cea.fr (M. Dubois).

0008-8846/00/$ – see front matter
PII: S0008-8846(99)00252-5

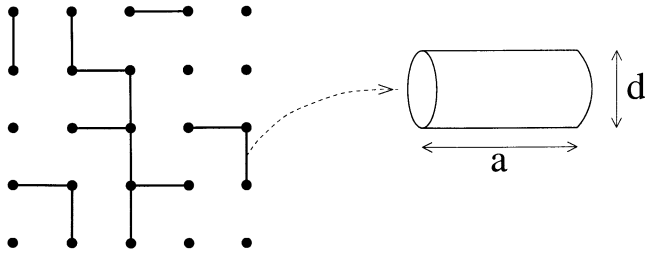

Fig. 1. A simple pore network model, representing one level of the hierarchical network. Sites (●) and pores (–) of non-null diameter. A pore has the form of a cylinder of length a and diameter d.

Works cited above establish the link between the MIP and the percolation process, but the simulation results are generally not directly comparable with the experimental data (except in some special cases such as sandstone). The major shortcoming of these models is that the possible correlations between neighbor pores are not taken in account. This approximation is not always satisfactory [10]. In fact in a number of materials (e.g., cement pastes, fractured rocks) porosity presents a hierarchical structure, which naturally introduces correlations between the pore length and the pore diameter. These correlations have an important influence on the MIP results. The correlations can be introduced by means of the fractional Brownian motion, as in Knackstedt and Sheppard's work [10], or by a construction of a hierarchical network [11,12]. The second possibility, used in the present work, has an advantage that a separate families of pores on different length scales are naturally obtained. The geometry of the network is relatively simple and the results can be easily understood.

In this article we focus on the interpretation of the MIP results obtained for hardened cement pastes (hcp). Two types of porosity can be distinguished in a cement paste: the porosity of the hydration product (C-S-H porosity) and the macroporosity (also called capillary porosity). Experiments show that the C-S-H porosity consists of two families of pores [13], which we denote micropores (typical diameter of 20 to 30 nm) and nanopores (typical diameter of 2 to 4 nm). These two families of pores can be interpreted as the porosity of outer and inner C-S-H. The outer C-S-H then would be the hydrates developed at the beginning of the hydration process, when their formation is not restricted by the geometrical constrains, and the inner C-S-H would be formed at the end of the hydration process. It should be mentioned that the microscopic organization of C-S-H pores still remains under investigation. Assumed to be an intrinsic property of the hydrates, the C-S-H porosity should not evolve with the water/cement (w/c) ratio [13]. The macroporosity includes all the pores having the diameters $d > 30$ nm. According to the Powers-Brownyard (PW) model [14], these pores are formed by the volume occupied by water that is not consumed during the hydration process, and hence it depends strongly on the w/c ratio. For w/c < 0.38 all the water is ultimately consumed, so there is no macroporosity present in the sample. It starts to develop only for w/c > 0.38 [14].

Our experimental MIP results do show a change of the pore size distribution with w/c ratio. Nevertheless, for the reasons cited above, an interpretation of this evolution is not straightforward. We developed a three-dimensional MIP simulator based on a multiscale percolation network [11,15], having three levels of hierarchy corresponding to the three families of pores. This model, described below, allows us to elucidate the relationship between the real and the measured pore size distributions. We study the change of this distribution under the variation of the porosity of macropores. The obtained results allow a correct interpretation of the experimental data.

2. Description of the model

Take a regular cubic network of L^3 sites. A two-dimensional section of such a network is represented in Fig. 2a. Let a be the distance between two nearest neighbor sites (grid size). A pair of neighbor sites i, j is connected by a cylinder-shaped pore of a diameter d_{ij}, which is randomly drawn from a distribution $f(d)$ [see Eq. (2)]:

$$f(d) = (1-p)\delta(d) + pg(d), 0 \leqslant p \leqslant 1 \quad (2)$$

where $\delta(d)$ is a delta distribution and $g(d)$ is a strictly positive distribution. Consequently, a fraction $(1 - p)$ of pores has a null diameter. The parameter p fixes the network connectivity.

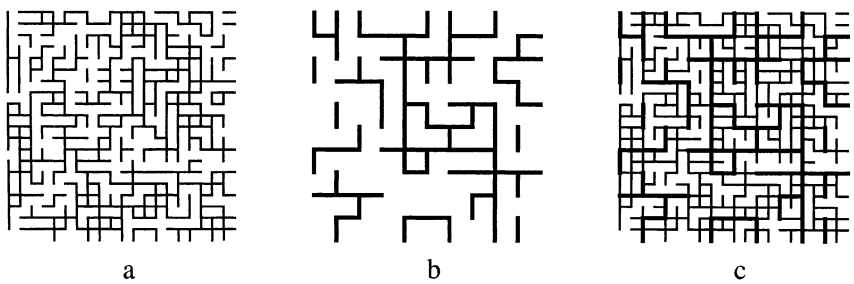

Fig. 2. Construction of the hierarchical network with $H = 2$ levels of hierarchy with the scaling factor $b = 2, p_1 = 0.6, p_2 = 0.4$. (a) One-level network with the grid size a_1; (b) one-level network with the grid size $a_2 = 2a_1$; (c) the hierarchical network after the superposition of (a) and (b).

Let the network described above represent the first level of a hierarchical pore structure. It is fully determined by the parameters L, a_1, and p_1 and by the distribution $g_1(d)$. A hierarchical network with two levels is created by the superposition of this network to a similar network with the grid size a_2, where a_2 is a multiple of a_1 ($a_2 = ba_1$), and with a pore size distribution $f_2(d) = (1-p_2)\delta(d) + p_2 g_2(d)$. This process is illustrated in Fig. 2. By definition, pores on the first level covered during the superposition by the pores of the second level disappear.

The basic length scale of the hierarchical network is the grid size a_1. It is thus natural to decompose each pore on the level 2 into b segments of the length a_1. Now two nearest neighbor sites in the original network are connected by a segment of a pore; the diameter of a segment connecting sites i, j is denoted d_{ij}. A pore segment will be called "accessible" if it is connected to one of the faces of the network by an uninterrupted path of segments. The set of such segments is denoted Ω. The volume of a segment being $v_{ij} = \pi d_{ij}^2 a_1/4$, the volume of accessible pore space V_0, is calculated as $V_0 = \Sigma_\Omega v_{ij}$.

The algorithm of the MIP simulations reflects the experimental procedure. It is similar to the algorithm used in the case of invasion percolation [16,17]. The network is "immersed" in mercury, which is allowed to enter the pore space from all the faces. From Eq. (1) a pore diameter d is associated to each pressure P, so that only the pores with $d' \geqslant d$ can be invaded. If a pore is invaded at a given pressure P, its neighbors with the diameter $d' \geqslant d$ are also invaded. We measure the intruded volume $V_i(d)$ under the pressure $P(d)$.

Let $V(d)$ be the cumulative volume of accessible pores in the sample, having the diameters $d' > d$. For the interpretation of our simulations we use a function $\Psi(d)$, defined as

$$\Psi(d) = \frac{dV(d)}{d(\ln d)} \tag{3}$$

$\Psi(d)$ is defined as a logarithmic derivative rather than a normal derivative, because then it allows comparison of the porosity of two pore families with very different characteristic diameters: $\epsilon\Psi(d)$ gives the fraction of the total accessible pore volume V_0 due to pores being in the diameter interval $(d; d + \epsilon d)$ rather than in the interval $(d; d + \epsilon)$. As discussed in the introduction, due to the existence of hidden pores the intruded volume $V_i(d)$ under a pressure $P(d)$ is generally different from $V(d)$. Then the measured pore size distribution $\Psi(d)$ [defined through the logarithmic derivative of $V_i(d)$] will be also different from the real distribution $\Psi(d)$. The aim of this section is to find the relationship between $\Psi(d)$ and $\Psi_i(d)$ in hierarchical networks as a function of the porosity.

The distribution $\Psi(d)$ [or $\Psi_i(d)$] is defined as a continuous function of the diameter [Eq. (3)]. In experiments, the intruded volume is not measured continuously, but a discrete sampling is used. Generally we take a set of pressures $\{P_0, P_1 \ldots P_{max}\}$ distributed over a logarithmic scale ($P_{i+1} = aP_i$, where a is a chosen constant) and the intruded volume is measured for each of these pressures. The same procedure is used in the simulations, but instead of working with the pressures, we work directly with a set of corresponding diameters ($d_0, d_1, \ldots d_{min}$). Plotted function $\Psi_i(d)$ is than evaluated as shown in Eq. (4)

$$\Psi_i\left(\frac{d_i + d_{i+1}}{2}\right) = \frac{V_i(d_i) - V_i(d_{i-1})}{\ln(d_i/d_{i-1})} \tag{4}$$

We use a similar sampling frequency as in real experiments. Because of the computer limitations, we work with a networks of "moderate" sizes: $L = 40$ (40^3 sites) in the case of one-level network and $L = 80$ in the case of hierarchical network. Then the ratio of the maximum pore size to the sample size is much smaller for the simulations (20–40) than in the case of real experiments ($\sim$ 1,000). The finite size effects resulting from this choice are discussed in detail below.

Assuming that the pore size distribution is described by Eq. (2), the porosity can be varied by changing either p or $g(d)$. The implications of changing $g(d)$ under the fixed connectivity p are rather trivial. We thus focus on the less trivial case, where the pore size distribution of the pores of non-null diameter $g(d)$ is fixed, and only the connectivity of the network varies. As we look only for a qualitative correspondence between our model and the cement paste (we cannot pretend to obtain a good quantitative description with a pore-network model), the choice of the length scale and precise form of $g(d)$ have a little importance. For simplicity we assume that $g(d)$ is a Gaussian distribution with mean m and variance σ, truncated for $d < 0$. If $(\sigma/m)^2 << 1$, we have approximately $g(d) \simeq 1/\sqrt{2\pi\sigma^2}\exp[-(d-m)^2/2\sigma^2]$. The main part of the porosity is then due to pores of the diameter $d_M = \sqrt{\langle d^2 \rangle} = \sqrt{m^2 + \sigma^2}$.

3. Simulation results

For better understanding of the dependence of MIP results on the connectivity of the pore space, we first examine the case of a simple one-level network with $m = 1$ and $\sigma = 0.2$. The distributions $\Psi_i(d)$ obtained for different values of p are shown together with $\Psi(d)$ in Fig. 3. We remark the existence of a critical diameter d_c (or equivalently of a critical pressure P_c). For $P < P_c$, the volume of invaded pore space is very small, even if the porosity created by pores having a diameter $d > d_c$ is not negligible, because smaller pores on the surface block the access of the liquid into bigger pores in the bulk of the network. The part of the peaks present for $d > d_c$ is only due to the finite size effects. If the size of the network grows, the surface/volume ratio goes to zero and the fraction of porosity invaded for $P < P_c$ vanishes (Fig. 4). The bulk is invaded only at P_c; the network of invaded pores forms for the first time a percolating cluster

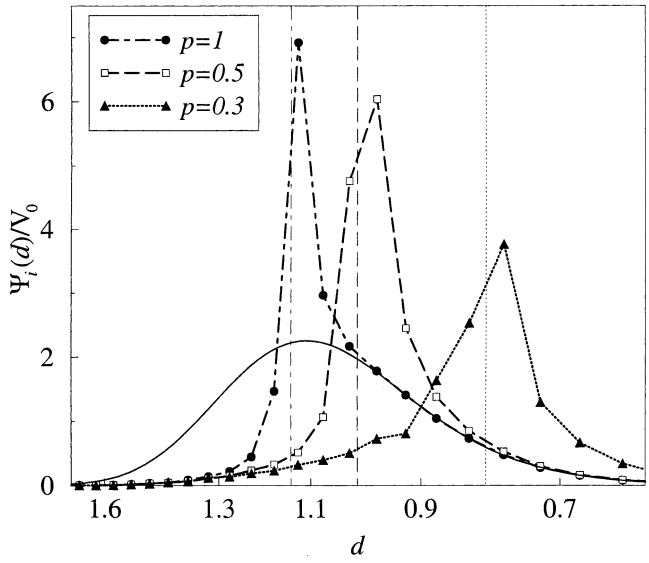

Fig. 3. Results of the simulations of the mercury porosimetry intrusion in the network with the Gaussian distribution of pore diameters ($m = 1, \sigma = 0.2$). Results for $p = 1$(●), $p = 0.5$(□), and $p = 0.3$(▲). The values of d_c obtained from Eq. (5) are shown, respectively, with dot-dashed, long-dashed, and dotted thin lines. The real pore size distribution $\Psi(d)$ is shown by bold solid line. $\Psi(d)/V_0$ does not depend on p.

[8]. Hence the critical diameter is related to the percolation threshold p_c of the network by the relation seen in Eq. (5) [18]

$$\int_{d_c}^{\infty} g(x)dx = \frac{p_c}{p} \tag{5}$$

For the cubic bond percolation network it is known that $p_c \sim 0.249$ [19]. As the bulk is already invaded for $P > P_c$, an important fraction of pores is directly connected to the percolating cluster of invaded pores, so $\Psi_i(d)$ converges rapidly toward $\Psi(d)$. In a very narrow region around d_c this convergence is algebraic [8]. Our numerical results indicate that out of this critical region $\Psi_i(d)$ converges to $\Psi(d)$ exponentially (inset A in Fig. 4). This convergence is related to the distribution of isolated clusters of pores having the diameter $d > d_c$. This explains the fact that the convergence is slower for weekly connected networks, where the probability of existence of isolated clusters is higher (see Fig. 3). As shown by the previous analysis, MIP results indicate a nonzero porosity only once invaded pores form a percolating cluster. Information about the pore size distribution of pores having $d > d_c$ is *not* accessible by this method. Another important point is that the value of d_c, corresponding roughly to the peak of $\Psi_i(d)$, can be different from d_M [the peak of $\Psi(d)$]. For the low connectivity networks, d_c is significantly lower than d_M.

Now we return to the hierarchical network. We choose a network with three hierarchical levels, corresponding to the three families of pores in cement pastes. For simplicity we assume that the scaling factor value is $b = 2$. The case of higher values of b will be discussed at the end of this section. The distribution of pore diameters on each level is given again by Eq. (2). Let the parameters of $g(d)$ on each level be, respectively, $m_1 = 1, \sigma_1 = 0.2$; $m_2 = 2, \sigma_2 = 0.4$; and $m_3 = 4, \sigma_3 = 0.8$. We obtain three distinct families of pores having typical diameters $d_M = 1.02, 2.04$, and 4.08. MIP peaks corresponding to these families are denoted by Roman numbers I, II, and III. The connectivity and the porosity of the network are determined by the triplet (p_1, p_2, p_3).

The results are shown in Fig. 5. The connectivity, as well as the porosity, are maximum if $p_1 = p_2 = p_3 = 1$—case(1; 1; 1). This corresponds to a high w/c ratio. As w/c decreases, the porosity of macropores decreases as well, which is simulated by decreasing the value of p_3—case (1;1;0.5). Peak III evolves similarly as the isolated peak

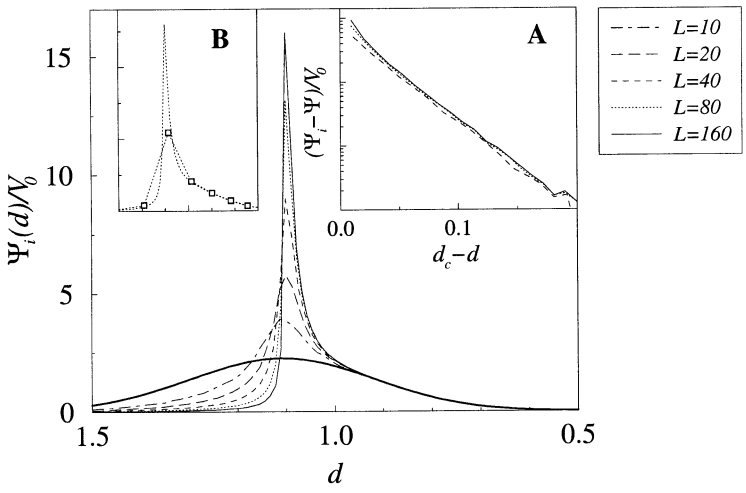

Fig. 4. Results of the MIP simulations in the network with the Gaussian distribution of pore diameters ($m = 1, \sigma = 0.2$). Results for the networks of the size between 10^3 and 160^3 sites. $\Psi(d)$ with a thick solid line. Inset A: Exponential convergence of $\Psi_i(d)$ toward $\Psi(d)$ for $d < d_c$ (linear-logarithmic plot). To present clearly the effects of the finite size, the frequency of sampling used in these simulations was much higher than in real experiments. The effects of sampling frequency are seen in inset B.

studied above: its position moves toward the smaller diameters. Next, we decrease both the values of p_2 and p_3, which allows us to study the behavior of the MIP results if the connectivity of micropores is lowered as well—case (1;0.5;0.3). Peak III continues to shift toward the smaller diameters, but the position of peak II is unchanged. In fact as macropores still form the percolating cluster, the network of micropores is always well connected through the macropores, so the variation of p_2 has no effect on the position of peak II. Last, the connectivity of all pore families is decreased—case (0.8;0.4;0.1). The value of p_3 is now below the percolation threshold. Macropores do not form a percolating cluster and so peak III disappears. Peak II becomes the leftmost peak, so it moves toward the smaller diameters and the position of peak I does not change. It is thus seen that (with the exception of the leftmost peak) the positions of the peaks on the MIP results do not depend on the connectivity, so it indicates the correct diameter of the corresponding pore class. The diameter indicated by the leftmost peak can be underestimated.

In Fig. 6 we plot $\Psi_i(d)$ and $\Psi(d)$ for the case (0.8;0.4;0.1), which allows comparison of the real and the measured porosity corresponding to a given family of pores. The porosity indicated by the leftmost peak (peak II) is clearly overestimated, because the porosity of macropores that do not form a percolating cluster appears as a part of this peak. The estimation furnished by the second peak from the left (peak I in this case) is already reasonable.

The preceding results were obtained for the network with the scaling factor $b = 2$, which corresponds to the case where the length scales of neighbor families of pores are close. The analysis is different if $b >> 2$. This case is

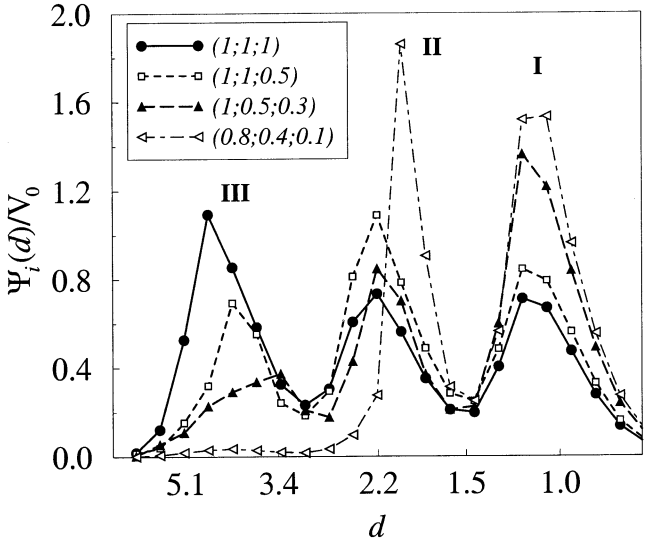

Fig. 5. Results of the MIP simulations on the hierarchical network with three levels, $b = 2$. The parameters of the pore size distribution are $m_1 = 1, m_2 = 2, m_3 = 4, \sigma_1 = 0.2, \sigma_2 = 0.4, \sigma_3 = 0.8$. $\Psi_i(d)$ with p_1, p_2, p_3 equal respectively to 1.0, 1.0, 1.0 (●); 1.0, 1.0, 0.5 (□); 1.0, 0.5, 0.3 (▲); 0.8, 0.4, 0.1 (◁).

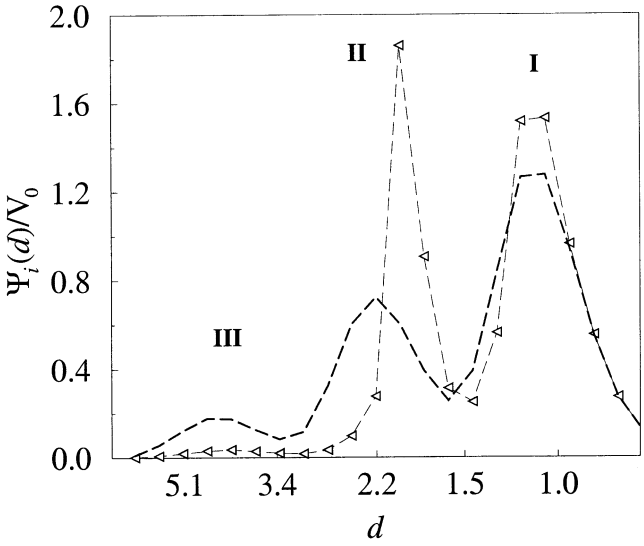

Fig. 6. Comparison of $\Psi_i(d)$ (◁) with $\Psi(d)$ (dot-dashed thin line without symbols) with $(p_1, p_2, p_3) = 0.8, 0.4, 0.1$.

not accessible for the simulations because of the computer limitations; nevertheless, the behavior can be deduced from the preceding results. The pores on the level i will occupy large regions that are not intersected by the pores of larger diameter (level $i' > i$). Hence the percolation-like effects, observed on the one level network (Fig. 3), will affect all families of pores. Then the position of each peak will evolve independently with the connectivity of the corresponding pore class.

In the cement paste, the ratio of typical diameters of neighbor pore classes is of the order of 5 to 10 (Fig. 7), so the question of the significance of results obtained with a network with $b = 2$ arises. It must be stressed that b is the

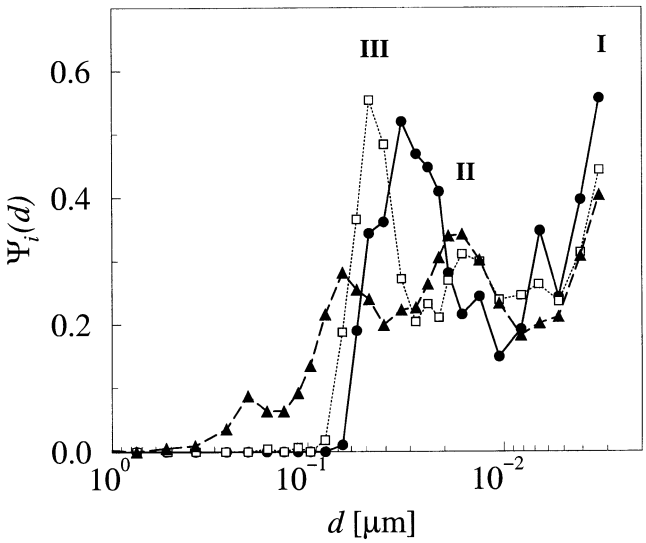

Fig. 7. Experimental results of the MIP in CEM I pastes. w/c = 0.5 (▲), w/c = 0.4 (□), w/c = 0.3 (●).

ratio of the length scales, which can be generally different from the ratio of the typical diameters. Moreover, as it is seen on experimental MIP results, neighbor peaks are not separated [$\Psi_i(d) > 0$ between two peaks], which suggest that the length scales of neighbor families of pores are not separated either. From this point of view the network with $b = 2$ better represents the structure of the cement paste than the network with $b >> 2$.

4. Interpretation of experimental data

Pore size distributions were measured on hardened cement pastes (hcp). Two cements were selected: CEM I (ordinary Portland cement) and CEM V (blended cement with slag and ashes). Materials were cured underwater during an average period of 30 months. After curing, hcp were freeze-dried for MIP tests [20].

In Fig. 7 we plot the pore size distributions obtained for the CEM I hcp with $w/c = 0.3, 0.4$, and 0.5. For $w/c = 0.4$ and 0.5 two marked peaks are visible: the macroporosity peak (peak III) and the microporosity peak (peak II). Since the characteristic diameter of the third family of pores is too small, only the beginning of the nanoporosity peak is visible (peak I). With decreasing w/c the position of peak III shifts toward smaller diameters. From the analysis of the volumes of the capillary porosity we deduce that the main reason for this displacement is *not* an average decrease in the pore diameters, but the decrease in the connectivity of the pore space. For $w/c = 0.5$ the capillary porosity is divided into two peaks: a small peak around $d \simeq 200$ nm with corresponding volume $v_1 = 0.0045\ \mathrm{mLg}^{-1}$ and a marked peak around $d \simeq 80$ nm with corresponding volume $v_2 = 0.044\ \mathrm{mLg}^{-1}$. For $w/c = 0.4$ the capillary porosity is concentrated in one peak centered around $d \simeq 50$ nm with corresponding volume $v_3 = 0.036\mathrm{mLg}^{-1}$. Under the hypothesis that the structure of the pore space does not evolve between $w/c = 0.5$and0.4 and that only the diameter of the capillary pores changes, it is possible to evaluate approximately the volume of the capillary pores for $w/c = 0.4$ from the results at $w/c = 0.5$. If the diameter of the capillary pores decreases from 200 and 80 nm to $d \simeq 50$ nm, the volume of the capillary pores for $w/c = 0.4$ is given by $v \simeq (50/200)^2 v_1 + (50/80)^2 v_1 \simeq 0.017\ \mathrm{mLg}^{-1}$. This value is much smaller than v_3 obtained by the MIP. Hence the diameter of capillary pores measured by MIP is underestimated, with the peak being shifted to the right due to the small connectivity of the pore space.

It is interesting to note that peak III is visible even for $w/c = 0.3$. It shows that there exists a macroporosity in the sample even for $w/c < 0.38$, which seems to be in disagreement with the Powers-Brownyard model of hydration. As discussed elsewhere [21], the macroporosity is not necessarily formed by water in excess, but it can be also a product of self-desiccation. The authors claim that there exists a point of the hydration process behind which macroporosity no longer forms a percolating cluster. Then, even if the sample is cured under water, the relative humidity in the isolated cavities decrease, which results in the formation of macropores. Nevertheless, it must be pointed out that because the macroporosity peak is present on the MIP results, macropores *do* form a connected cluster throughout the sample [see the discussion around Eq. (4)]. This shows that the macroporosity is not only a result of self-desiccation.

The position of peak II does not evolve with w/c, only its amplitude does. This is in accordance with observation that the hydration process can lead to several characteristic morphologies of the pore space (for example outer and inner C-S-H) [14]. The morphology does not evolve continuously with w/c; only a fraction of C-S-H corresponding to a given morphology varies.

The results for the CEM V pastes are presented in Fig. 8. The peak III is absent. It starts to develop only for $w/c = 0.5$, which shows that the percolation threshold of the capillary porosity is much higher for CEM V than for the CEM I paste. This observation conforms to theoretical predictions [22]. The leftmost peak then corresponds to the C-S-H porosity (peak II). For $w/c = 0.5$ it has exactly the same position as for CEM I pastes (see the inset in Fig. 8), which indicates that the morphology of C-S-H hydrates is the same in both cases. The position peak II moves toward the smaller diameters as w/c decreases, which is clearly an artifact due to small connectivity effects: as shown in the CEM I case, morphology does not evolve continuously with w/c, but it is fixed by the hydration process. As well as in the CEM I hcp case, the fraction of the porosity formed by outer C-S-H decreases with w/c.

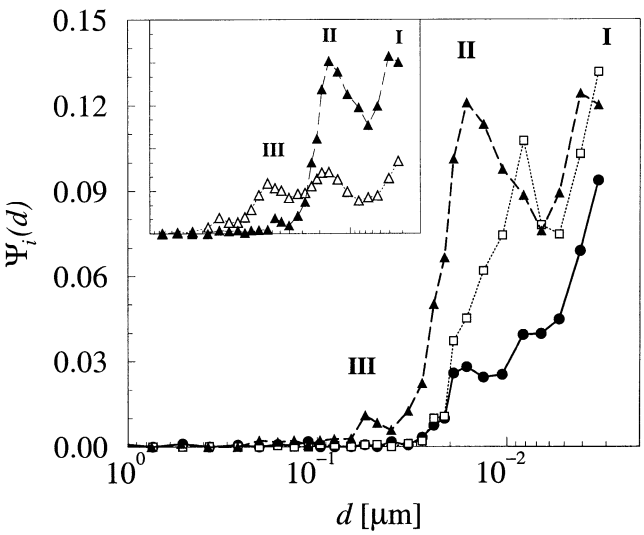

Fig. 8. Experimental results of the MIP in CEM V pastes. $w/c = 0.5$ (▲), $w/c = 0.4$(□), $w/c = 0.3$(●). In the inset comparison of the results for CEM I (△) and CEM V (▲) for $w/c = 0.5$.

The pore size distribution changes drastically if a reactive mineral admixture is added to the pure paste, even if formed hydrates are the same in both cases. The difference is probably due to the dynamics of the hydration process. Slag and ashes form the hydrates through reaction with the Portlandite. This reaction can proceed only once the hydration of C_3S and C_2S have started. The hydration is then slower and the organization of hydrates is different in CEM V than in the pure hcp case.

5. Conclusion

We have developed a MIP simulator that takes into account the hierarchical structure of the porosity of cement pastes. We have shown that the position of peak III, corresponding to the family of pores with the biggest diameters, depends not only on the real diameter of these pores but also on the connectivity of this pore class in the sample: as connectivity decreases, the position of the peak shifts toward smaller diameters. The position of the other peaks does not evolve if the connectivity is changed. Similarly, the porosity indicated by the leftmost peak is overestimated, since it includes the porosity created by macropores that do not form themselves a percolating cluster. The other peaks furnish a reasonable estimation of the porosity of the corresponding pore family. These results clearly indicate the limitations of the MIP technique and they allow for a correct interpretation of the MIP data. We have interpreted MIP data obtained for the CEM I and CEM V cement pastes. Experimental data show that in the CEM I case a *connected* capillary porosity is present even for $w/c = 0.3$. Remember that our samples were cured for a period of 30 months, so a complete hydration should be achieved. Moreover, the fact that the macroporosity is connected seems to rule out the hypothesis that it is formed as a consequence of the self-desiccation. This result is rather surprising, because it is at variance with the Powers-Brownyard model of hydration. The addition of reactive mineral admixture raises the percolation threshold of the capillary porosity, which raises up to w/c = 0.5 for CEM V paste. MIP results are in accordance with observations that the hydration process determines the morphology of the hydration product, which is then fixed and does not evolve with w/c. The morphology of C-S-H corresponding to pores accessible by MIP ($d > 3$ μm) seems to be the same for the pastes with and without reactive admixture.

References

[1] W.K. Bell, J. van Brakel, P.M. Heertjes, Mercury penetration and retraction hysteresis in closely packed spheres, Powder Tech 29 (1981) 75.
[2] E.J. Garboczi, Mercury porosimetry and effective networks for permeability calculations in porous materials, Powder Tech 67 (1991) 121.
[3] I. Fatt, The network model of porous media, Trans AIME 207 (1956) 144.
[4] J. Koplik, S. Redner, D. Wilkinson, Transport and dispersion in random networks with percolation disorder, Phys Rev A 37 (1988) 2619.
[5] M. Sahimi, Flow phenomena in rocks From continuum models to fractals, percolation, cellular automata, and simulated annealing, Rev Mod Phys 65 (1993) 1393.
[6] A.M. Lane, N. Shah, N. Wm.C. Conner, Measurement of the morphology of high-surface-area solids. Porosimetry as a percolation process, J Col Int Sci 109 (1986) 235.
[7] C.D. Tsakiroglou, A.C. Paytakes, A new simulator for mercury porosimetry for the characterization of porous materials, J Coll Int Sci 137 (1990) 315.
[8] D. Stauffer, A. Aharony, Introduction to Percolation Theory, Taylor & Francis, Washington, D.C. 1992.
[9] R.G. Larson, N.R. Morrow, Effects of sample size on capillary pressures in porous media, Powder Tech 30 (1981) 123.
[10] M.A. Knackstedt, A.A. Sheppard, Simulation of mercury porosimetry on correlated grids Evidence for extended correlated heterogeneity at the pore scale in rocks, Phys Rev E 58 (1998) 6923.
[11] A.V. Neĭmark, Multiscale percolation systems, Sov Phys JETP 69 (1989) 786.
[12] P. Gavrilenko, Y. Guéguen, Flow in fractured media A modified renormalisation method, Water Resource Research 34 (1998) 177.
[13] V. Baroghel-Bouny, Caractérisation des pates de ciment et des bétons, Laboratoire Central des Ponts et Chaussées, 1994.
[14] H.F.W. Taylor, Cement Chemistry, Academic Press, New York, 1990.
[15] K. Xu, J.-F. Daian, D. Quenard, Multiscale structures to describe porous media. Part I Theoretical background and invasion by fluids, Transp Porous Media 26 (1997) 51.
[16] D. Wilkinson, J.F. Willemsen, Invasion percolation: A new form of percolation theory, J Phys A 16 (1983) 3365.
[17] J.-N. Roux, D. Wilkinson, Resistance jumps in mercury injection in porous media, Phys Rev A 37 (1988) 3921.
[18] A.J. Katz, A.H. Thompson, Quantitative prediction of permeability in porous rock, Phys Rev B 34 (1986) 8179.
[19] D.G. Gingold, C.J. Lobb, Percolative conduction in three dimensions, Phys Rev B 42 (1990) 8220.
[20] C. Gallé, J.-F. Daian, M. Pin, Transfert des gaz dans les matériaux cimentaires: Expérimentation et modélisation du couplage microstructure/saturation en eau/perméabilité, Compte-rendu des journées techniques AFPC-AFREM, Durabilité des Bétons, Toulouse, France, 11-12 Décembre, 1997.
[21] D.P. Bentz, K.A. Snyder, P.E. Stutzman, Hydration of Portland cement The effects of curing conditions, in: H. Justnes (Ed.), Proceedings of the 10th International Congress on the Chemistry of Cement, Vol. 2, Gothenburg, Sweden, Amarkai AB and Congrex Goteborg AB, 1997.
[22] D.P. Bentz, E.J. Garboczi, Percolation of phases in a three-dimensional cement paste microstructure model, Cem Concr Res 21 (1991) 325–344.